International Journal of Thermophysics, Vol. 27, No. 2, March 2006 (© 2006)
DOI: 10.1007/s10765-005-0010-5

Surface Tension Prediction Using Characteristics of the Density Profile Through the Interfacial Region

A. P. Wemhoff[1,2] **and V. P. Carey** [1]

Received February 14, 2005

A simple surface tension estimation technique is described that is based solely upon the characteristics of the density profile in the interfacial region and the physical properties of the molecules in the fluid. This method, denoted free energy integration (FEI), links interfacial tension to known interfacial region density profile characteristics obtained via experiment or simulation. The general FEI methodology is provided here, and specific relations are derived for a methodology that incorporates the Redlich–Kwong fluid model. The Redlich–Kwong based FEI method was used to predict interfacial tension using the density profile characteristics of molecular dynamics (MD) simulations of argon using the Lennard–Jones potential, diatomic nitrogen using the two-center Lennard–Jones potential, and water using the extended simple point-charge (SPC/E) model. These results for argon compare favorably to values calculated by the traditional virial approach, known values from the literature using the finite-size scaling technique, and ASHRAE recommended values. In addition, the FEI predictions agree well with ASHRAE values and predictions using the virial method for nitrogen for the simulated range of temperatures in this study, and for water for reduced temperatures above 0.7. In addition, the FEI method results agree well with other established theoretical techniques for predictions of the surface tension of sulfur hexafluoride close to the critical point.

KEY WORDS: interfacial region; molecular dynamics; Redlich–Kwong; surface tension.

1. INTRODUCTION

Surface tension is an important macroscopic thermophysical property of fluids that affects behavior in a variety of processes such as boiling heat

[1] Department of Mechanical Engineering, University of California, Berkeley, California 94720-1740, U.S.A.
[2] To whom correspondence should be addressed. E-mail: wemhoff2@llnl.gov

transfer [1], condensation [2], and microscale channel flow [3]. Two widely-used traditional means of deriving surface tension using computer simulations have previously been developed. The first method uses molecular dynamics (MD) simulations to determine the pressure tensor variation through the interfacial region [4], and the difference between the normal and tangential components of the pressure tensor across the interfacial region is integrated to attain the surface tension, γ,

$$\gamma = \int_{z=-\infty}^{z=+\infty} [P_{\mathrm{n}}(z) - P_{\mathrm{t}}(z)]\, dz \tag{1}$$

This approach is valid, since the interfacial tension comprises the only source of anisotropy in the pressure tensor. This method, commonly known as the virial method (or virial expression), has been used extensively to estimate surface tension values for argon (e.g., Weng et al. [5]), diatomic fluids (e.g., Enders et al. [6]), hydrocarbons (e.g., Harris [7]), and water (e.g., Alejandre et al. [8]). Nijmeijer et al. [9], Dunikov et al. [10], Holcomb et al. [11], and Mecke et al. [12] found that the intermolecular potential truncation method and distance impact the accuracy in calculating the surface tension using the virial method. Therefore, Barker [13] and Sinha et al. [14] added long-range corrective terms in the surface tension calculation to yield predictions of surface tension for argon in good agreement with ASHRAE recommended values [15].

Finite-size scaling [16–19] provides an attractive alternative method to surface tension prediction using a grand canonical Monte Carlo simulation, for the cutoff and domain size dependencies are incorporated into the model. In this method, the interfacial region is not simulated. Instead, the difference between the probability of observing bulk liquid and vapor states ($P_{\max}$) and the minimally probable intermediate state ($P_{\min}$) is used as a measure of the excess free energy due to the presence of the interfacial region for a known domain characteristic dimension. Comparison of several simulated excess free energy values at various domain sizes allows for extrapolation to the interfacial tension value corresponding to an infinite domain. This approach has the advantage over the virial approach since it has been established that the size of the domain has an effect on the interfacial region profile [20]. Nonetheless, Errington has shown that both methods provide good agreement under proper simulation conditions [17].

Various theoretical approaches are also available for estimation of surface tension. Brock and Bird [21] used a corresponding states method to estimate the surface tension variation with reduced temperature. Similarly, Carey [22] used a neoclassical theory of capillarity to estimate

this variation. In addition, Carey and Wemhoff [23] developed a closed-form solution using a Redlich–Kwong fluid model to estimate surface tension from a knowledge of the interfacial region thickness. Finally, in this paper we describe the free energy integration (FEI) method as a simplified variation of density functional theory [24] to compute the system net excess free energy by performing a numerical integration of the local free energy density. It is the goal of this study to evaluate the effectiveness of the Redlich–Kwong-based FEI method by comparing estimated values using this method to those using the aforementioned methods.

2. GENERAL FORM OF THE FREE ENERGY INTEGRATION TECHNIQUE

The underlying theory for the FEI model is that the free energy per unit surface area for the liquid–vapor interfacial region is higher than the extension of the values of the two bulk phases to the center of the interfacial region. The difference in the free energy values of these two systems is the interfacial tension, which is written mathematically as

$$\gamma = \int_{z=-\infty}^{0} (\psi(z) - \psi_{\mathrm{l}})\, dz - \int_{z=0}^{+\infty} (\psi_{\mathrm{v}} - \psi(z))\, dz \tag{2}$$

where $\psi(z)$ is the Helmholtz free energy density at a given position z in the interfacial region, and ψ_{l} and ψ_{v} are the bulk values of the free energy density in the liquid and vapor interfacial regions, respectively. Note that in Eq. (2) $\psi_{\mathrm{v}} > \psi_{\mathrm{l}}$, and the center of the interfacial region is set at $z = 0$, which is defined by

$$\int_{z=-\infty}^{0} (\rho_{\mathrm{l}} - \rho(z))\, dz = \int_{z=0}^{+\infty} (\rho(z) - \rho_{\mathrm{v}})\, dz \tag{3}$$

Evaluation of Eq. (2) requires calculation of the free energy density for all z in the interfacial region. Generally, the free energy density may be written as the summation of two terms,

$$\psi(z) = \psi_0[\rho(z), T] + \psi_1[\rho''(z), T] \tag{4}$$

where T is the local temperature, and ρ and ρ'' are the molecular number density and second derivative of the number density of the system at a location z. If local thermodynamic equilibrium is assumed, then the temperature is constant through the interfacial region. The local density is

approximated using the hyperbolic tangent profile imposed by the van der Waals theory of capillarity [25],

$$\rho(z) = \frac{1}{2}(\rho_l + \rho_v) + \frac{1}{2}(\rho_l - \rho_v)\tanh\left(\frac{2z}{\delta z_i}\right) \tag{5}$$

where ρ_l and ρ_v are the liquid and vapor densities, respectively, and δz_i is the thickness of the interfacial region;

$$\delta z_i = \frac{\rho_l - \rho_v}{\left.\frac{d\rho}{dz}\right|_{z=0}} \tag{6}$$

The center of the interfacial region in Eq. (5) is set at $z = 0$, and the symmetry of Eq. (5) coupled with the $z = 0$ definition of Eq. (3) allows for the approximation of the center of the interfacial region occurring at ρ_m, where

$$\rho_m = \frac{\rho_l + \rho_v}{2} \tag{7}$$

Although the profile of Eq. (5) is used here, it should be noted that other expressions for the density profile have been developed (e.g., Fisk and Widom [26], Buff et al. [27], Robert and Stuart [28], and Robert [29]). However, the FEI analysis has been found to be independent of the specific density profile used [30]. If the density profile is assumed to follow the proposed fit curve relation of Eq. (5), then the second derivative of the density profile is

$$\rho''(z) = \frac{4}{\delta z_i^2}(\rho_l - \rho_v)\,\mathrm{sech}^2\left(\frac{2z}{\delta z_i}\right)\tanh\left(\frac{2z}{\delta z_i}\right) \tag{8}$$

Evaluation of the local free energy density in Eq. (4) requires use of a prescribed fluid model that reasonably approximates the correct thermodynamic relations under metastable superheated liquid and supersaturated vapor fluid conditions. Although molecular models provide the most accuracy in estimating the free energy density, a general fluid model is advantageous in that it provides reasonable estimations to thermodynamic property values for a wide range of fluids. Several examples of these fluid models are known: van der Waals, Redlich–Kwong, Soave, and Peng–Robinson. Once the partition function Q of the fluid model is known, then the local free energy density can be calculated using the relation,

$$\psi = \frac{F}{V} = -\frac{k_B T}{V}\ln Q \tag{9}$$

Note that the partition function Q must include a curvature term allowing for the calculation of ψ_l in Eq. (4).

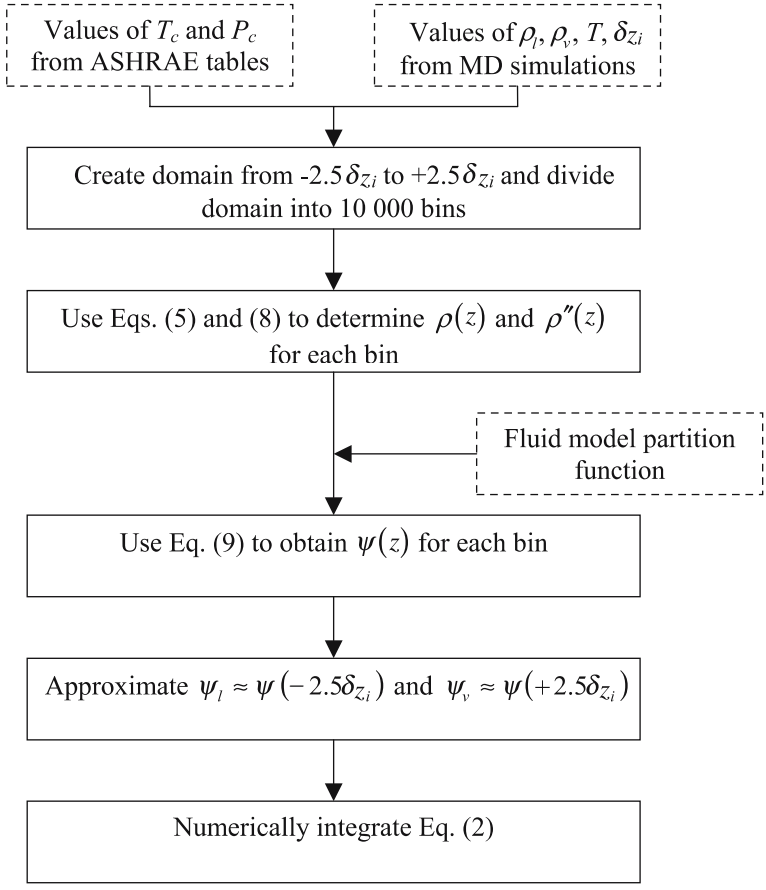

Fig. 1. Flowchart for general implementation of the FEI method.

Figure 1 shows the algorithm for performing the FEI technique. The user provides a fluid model and values of the fluid critical properties. In addition, the user supplies values of ρ_l, ρ_v, δz_i, and T, which may be acquired by either an MD simulation or an experiment. In the analysis, a domain is set up with a width that is five times the interfacial region thickness. This domain is divided into 10,000 bins of thickness Δz, and the local reduced molecular density is approximated in each bin using the density profile given by Eq. (5), where the value of z used in the calculation is located at the center of the bin. The local free energy density is calculated using Eq. (9). The bulk liquid and vapor free energy densities are approximated as those for the furthest negative and positive bins, respectively.

Then, the integration of Eq. (2) is performed numerically using basic block integration schemes.

3. FREE ENERGY INTEGRATION TECHNIQUE USING THE REDLICH–KWONG FLUID MODEL

The appendix provides the free energy density relation specific to the Redlich–Kwong fluid model. The Redlich–Kwong fluid model was utilized in this study, since it is generally more accurate than the van der Waals model in matching saturation data for a variety of fluids. The resultant expression for the local free energy density is

$$\psi = -\rho k_B T \left\{ \frac{3}{2} \ln \left[\frac{(1-\rho b_R)^{2/3}}{\rho^{2/3} \Lambda^2} \right] + F_1 \right\} - \frac{a_{R0} \ln(1+\rho b_R)}{b_R T^{1/2}} \times \left[\rho + L_i^2 0.08065 (1-T_r)^{-0.34} \rho'' \right] \tag{10}$$

where

$$\Lambda = \left[\frac{h^2}{2\pi M k_B T} \right]^{1/2} \tag{11}$$

and

$$F_1 = 1 + \frac{\xi - 5}{2} \ln\pi - \ln\sigma_s + \left(\frac{\xi - 3}{2} \right) \ln\left(\frac{T}{\theta_{rot,m}} \right) \tag{12}$$

where M is the molecular mass, a_{R0} and b_R are the Redlich–Kwong coefficients, k_B is Boltzmann's constant, h is Planck's constant, ξ is the number of degrees of freedom of the molecule, σ_s is the symmetry number, $\theta_{rot,m}$ is the rotational temperature of mode m, and

$$L_i = \left(\frac{k_B T_c}{P_c} \right)^{1/3} \tag{13}$$

In Eq. (10), F_1 and Λ are the only variables that depend on the physical characteristics of the molecules in the system. Table I lists the values of ξ, σ_s, and $\theta_{rot,m}$ for argon, nitrogen, and water, while Table II provides the values of F_1 for these fluids.

Equations (2), (5), (8), and (10) may be expressed in reduced form using the system critical parameters and the reduced properties:

$$\zeta = z/L_i \tag{14a}$$

Table I. Individual Geometric Factors for Each Fluid Type

Parameter	Description	Values		
		Argon	Nitrogen	Water
ξ	Molecular degrees of freedom	3	5	6
σ_s	Symmetry number	1	2	1
$\theta_{rot,m}$	Rotational temperature (K)	N/A	2.88	13.4, 20.9, 40.1

Table II. Values of the Factor F_1 for Each Fluid Type

Fluid	F_1
Argon	$1-2\ln\pi$
Nitrogen	$1-\ln(2)+\ln\left({}^{T}/_{2.88}\right)$
Water	$1+\ln\pi+1.5\ln\left({}^{T}/_{13.4}\right)\ln\left({}^{T}/_{20.9}\right)\ln\left({}^{T}/_{40.1}\right)$

$$\delta\zeta_i = \delta z_i / L_i \tag{14b}$$

$$b_r = b_R N_A / \hat{v}_c = 0.25992 \tag{14c}$$

$$a_r = a_{R0} N_A^2 / (P_c T_c^{1/2} \hat{v}_c^2) = 3.84732 \tag{14d}$$

$$a_{r,1} = a_{R0,1} N_A^2 / \left(P_c T_c^{1/2} \hat{v}_c^2 L_i^2\right) = 0.310286\,(1-T_r)^{-0.34} \tag{14e}$$

$$P_r = P / P_c \tag{14f}$$

$$T_r = T / T_c \tag{14g}$$

$$\rho_r = \hat{\rho} / \hat{\rho}_c \tag{14h}$$

$$v_r = \hat{v} / \hat{v}_c \tag{14i}$$

$$\gamma_r = \frac{\gamma}{P_c L_i} \tag{14j}$$

$$\psi_r = \frac{\psi}{P_c} \tag{14k}$$

$$\Lambda_r = \rho_c^{1/3}\Lambda = \rho_c^{1/3}\left[\frac{h^2}{2\pi M k_B T}\right]^{1/2} \tag{14l}$$

where Eqs. (14c) and (14d) use the compressibility of the Redlich–Kwong fluid at the critical point:

$$\frac{\rho_c k_B T_c}{P_c} = 3 \tag{15}$$

The resultant reduced form of Eqs. (2), (5), (8), and (10) are

$$\psi_r = -3\rho_r T_r\left\{\ln\left[\frac{1-\rho_r b_r}{\Lambda_r^3 \rho_r}\right] + F_1\right\} - \frac{\ln(1+\rho_r b_r)}{b_r T_r^{1/2}}\left[a_r\rho_r + a_{r,1}\frac{d^2\rho_r}{d\zeta^2}\right] \tag{16}$$

$$\gamma_r = \int_{\zeta=-\infty}^{0}\left(\psi_r(\zeta) - \psi_{r,l}\right)d\zeta - \int_{\zeta=0}^{+\infty}\left(\psi_{r,v} - \psi_r(\zeta)\right)d\zeta \tag{17}$$

$$\rho_r(\zeta) = \frac{1}{2}\left(\rho_{r,l} + \rho_{r,v}\right) - \frac{1}{2}\left(\rho_{r,l} - \rho_{r,v}\right)\tanh\left(\frac{2\zeta}{\delta\zeta_i}\right) \tag{18}$$

$$\rho_r''(\zeta) = \frac{4}{\delta\zeta_i^2}\left(\rho_{l,r} - \rho_{v,r}\right)\operatorname{sech}^2\left(\frac{2\zeta}{\delta\zeta_i}\right)\tanh\left(\frac{2\zeta}{\delta\zeta_i}\right) \tag{19}$$

Note that in Eqs. (16) through (19), the only unknown variables are the temperature, interfacial region thickness, bulk densities, and F_1. Furthermore, F_1 is known from Table II.

4. FEI SURFACE TENSION ESTIMATION COMPARED TO COMPUTATIONAL APPROACHES

In order to use the FEI method, values of the interfacial region thickness must be known. One means to obtain this thickness value is via MD simulations. In this study, MD simulations of argon, nitrogen, and water were run for a variety of system temperatures between $T_r = 0.60$ and $T_r = 0.85$. In the argon simulations, liquid molecules were initialized in a $6 \times 6 \times 9$ face-centered-cubic (fcc) lattice structure in the center of the

domain to create two interfaces. The lattice density matched the expected bulk liquid density from ASHRAE tables [15]. Vapor molecules were also placed in a fcc lattice structure, provided the lattice parameter was sufficiently small to fit in the simulation domain. The liquid region comprised approximately one-third of the simulation domain.

For argon, the molecular velocities were initialized corresponding to a low initial temperature ($T_r = 0.1$) following the methodology of Box and Mueller [31]. The configurations were updated each time step of 5 fs using the velocity Verlet algorithm [32]. The temperature of the system was then slowly raised to the desired equilibrium temperature via velocity rescaling for 20,000 steps, maintained at that temperature for 10,000 steps, and allowed to equilibrate for 10,000 steps prior to data collection. Argon molecules interacted via the Lennard–Jones potential,

$$\phi_{ij} = 4\varepsilon \left[\left(\frac{\sigma}{r_{ij}} \right)^{12} - \left(\frac{\sigma}{r_{ij}} \right)^{6} \right] \tag{20}$$

with parameters $\sigma = 0.34\,\text{nm}$ and $\varepsilon = 121\,k_B\,\text{K}$. The intermolecular potential and force between molecules i and j were smoothly truncated at the cutoff distance of one-half of the minimum simulation domain dimension (approximately 5.0 σ). Upon equilibration, the simulation domain was divided into 100 bins for data collection, and the mean density values were calculated over the final 160,000 time steps according to

$$\langle \rho \rangle = \frac{\langle N_{\text{bin}} \rangle}{V_{\text{bin}}} \tag{21}$$

where $\langle \rho \rangle$ is the mean molecular density, $\langle N_{\text{bin}} \rangle$ is the mean number of molecules in the bin, and V_{bin} is the bin volume. The authors have shown that 100 collection bins are sufficient to provide reasonable estimates of the interfacial region density profile position and thickness for the systems used in this study [30]. The surface tension was also calculated using a modified form of the virial method of Eq. (1),

$$\gamma = \frac{1}{2} \int_{-\infty}^{+\infty} (P_n - P_t)\, dz \tag{22}$$

where the factor of 1/2 stems from the presence of two interfaces in the simulation domain. The local normal and tangential pressure components were calculated by [33]

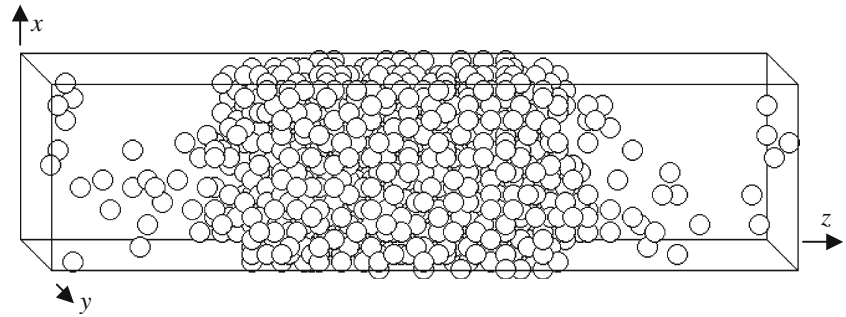

Fig. 2. Equilibrium simulation domain for argon, $T_r = 0.74$.

$$P_n = \frac{1}{V}\sum_{i=1}^{N} M_i v_{i,z}^2 + \frac{1}{V}\sum_{i=1}^{N}\sum_{j>i}^{N} F_{ij,z} z_{ij}$$
$$P_t = \frac{1}{2V}\sum_{i=1}^{N} M_i \left(v_{i,x}^2 + v_{i,y}^2\right) + \frac{1}{2V}\sum_{i=1}^{N}\sum_{j>i}^{N} \left(F_{ij,x} x_{ij} + F_{ij,y} y_{ij}\right) \tag{23}$$

Figure 2 provides a snapshot of the equilibrium configuration for 1296 argon molecules at a reduced temperature of 0.74. Figure 3 shows that the mean mass density profile calculated for argon at $T_r = 0.74$ compares well to the fit curve relation of Eq. (5). The application of the fit curve for a particular density profile may be performed by taking the gradient of the density using the two bins straddling the mean density value of the system using Eq. (7) and plugging this value into Eq. (6) to obtain the interfacial region thickness. The fit curve relation may alternately be found by manually iterating the value of the interfacial region thickness until it closely matches the bin data. The fit curve relation also matches data for the nitrogen and water systems with the same accuracy as that for argon. It should be noted that the simulated bulk density values were used in the FEI model, and the simulated bulk liquid density values generally deviated from ASHRAE data with an error less than 3%.

The nitrogen and water molecules followed the same initialization procedure as the argon molecules with some exceptions. The fcc liquid lattice was $6 \times 6 \times 6$ cells for nitrogen and $6 \times 5 \times 5$ cells for water. The translational velocities of the molecules were initialized in the same manner as for the argon system, but an initial angular velocity distribution was also applied that matched the Boltzmann rotational energy distribution function [34];

$$f(\varepsilon_{rot})\, d\varepsilon_{rot} = \frac{2\sqrt{\varepsilon_{rot}}}{\sqrt{\pi}\,(k_B T)^{3/2}} e^{-\varepsilon_{rot}/k_B T}\, d\varepsilon_{rot} \tag{24}$$

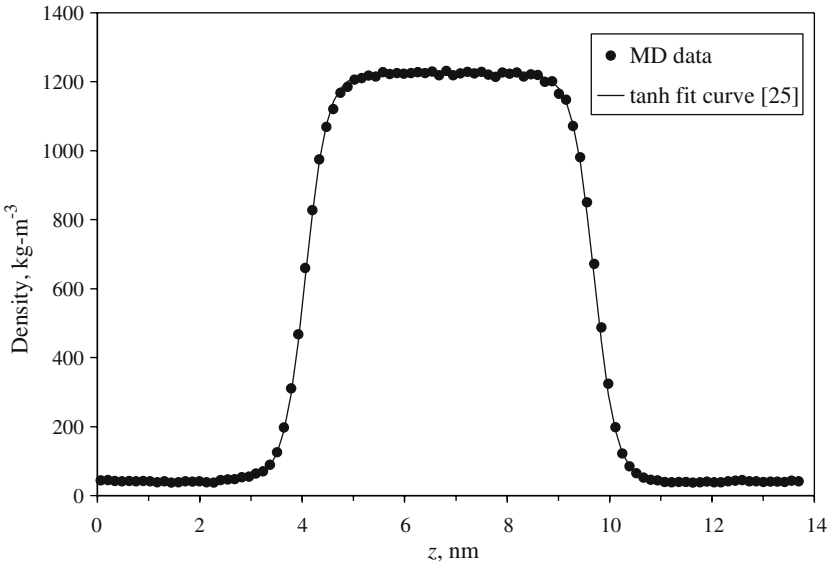

Fig. 3. Mean mass density profile for argon, $T_r = 0.74$.

where $f(\varepsilon_{\text{rot}})\, d\varepsilon_{\text{rot}}$ is the number of molecules with rotational energies between ε_{rot} and $\varepsilon_{\text{rot}} + d\varepsilon_{\text{rot}}$. The nitrogen system was equilibrated via velocity rescaling for 20,000 steps, and allowed to settle for an additional 20,000 steps, while these values were 15,000 steps and 5000 steps for water. For the polyatomic simulations, the molecular configuration was updated every time step using the RATTLE [35] algorithm, and the time step used was 1 fs.

The nitrogen molecules interacted via the two-centered Lennard–Jones potential function, where each nitrogen atom interacted with all atoms on other molecules with the potential given by the Lennard–Jones interaction of Eq. (20), where $\sigma = 0.33078$ nm and $\varepsilon = 36.673\, k_B$ K, and the nitrogen–nitrogen bond length is fixed at 0.1089 nm [36]. The potential and force interactions of these Lennard–Jones interatomic interactions were smoothly truncated at approximately 5.0 σ. The water molecules interacted via the SPC/E potential [37],

$$\phi_{ij} = 4\varepsilon \left[\left(\frac{\sigma}{r_{\text{OO}}} \right)^{12} - \left(\frac{\sigma}{r_{\text{OO}}} \right)^{6} \right] + \frac{1}{4\pi\varepsilon_0} \sum_{a=1}^{3} \sum_{b=1}^{3} \frac{q_a q_b}{r_{iabj}} \tag{25}$$

where r_{OO} is the oxygen–oxygen separation distance, ε_0 is the permittivity of a free vacuum, r_{iabj} is the radial distance between atom a of

molecule i and atom b of molecule j, and q_a and q_b are the values of the point charges on atoms a and b, respectively. In the SPC/E potential, the OH bond length is 0.100 nm, the HOH bond angle is 109.47°, and the oxygen atoms contain Lennard–Jones parameters σ and ε with values of 0.3166 nm and 78.21 k_B K, respectively. The oxygen and hydrogen point charges q_O and q_H are $-0.8476e$ and $+0.4238e$, respectively. The Coulombic interactions were truncated via the Ewald summation technique, where formulae are provided by Heyes [38] and Alejandre et al. [8],

$$U = \frac{1}{4\pi\varepsilon_0} \left\{ \begin{array}{l} \frac{2\pi}{V} \sum\limits_{\mathrm{k}\neq 0} Q(k) \left|S(\mathrm{k})\right|^2 + \sum\limits_{i=1}^{N} \sum\limits_{a=1}^{N_{\mathrm{atom}}} \sum\limits_{j>i}^{N} \sum\limits_{b=1}^{N_{\mathrm{atom}}} \frac{q_{ia}q_{jb}}{r_{iajb}} \mathrm{erfc}\left(\kappa r_{iajb}\right) \\ -\frac{\kappa}{\sqrt{\pi}} \sum\limits_{i=1}^{N} \sum\limits_{a=1}^{N_{\mathrm{atom}}} q_{ia}^2 - \frac{1}{2} \sum\limits_{i=1}^{N} \sum\limits_{a=1}^{N_{\mathrm{atom}}} \frac{q_{ia}q_{jb}}{r_{iaib}} \mathrm{erf}\left(\kappa r_{iaib}\right) \end{array} \right\} \tag{26}$$

where

$$S(\mathbf{k}) = \sum_{i=1}^{N} \sum_{a=1}^{N_{\mathrm{atom}}} q_{ia} \exp\left(i\mathbf{k} \bullet \mathbf{r}_{ia}\right) \tag{27}$$

and

$$Q(\mathbf{k}) = \frac{1}{k^2} \exp\left(-\frac{k^2}{4\kappa^2}\right) \tag{28}$$

The vector $\mathbf{k}$ is the reciprocal lattice vector and is denoted as

$$\mathbf{k} = \frac{2\pi n_x}{L_x}\hat{\mathbf{x}} + \frac{2\pi n_y}{L_y}\hat{\mathbf{y}} + \frac{2\pi n_z}{L_z}\hat{\mathbf{z}} \tag{29}$$

where n is the number of lattice points in a given direction, L is the dimension of the simulation domain, and $\hat{\mathbf{x}}, \hat{\mathbf{y}}$, and $\hat{\mathbf{z}}$ are Cartesian unit vectors. The value of κ was $5.6/L_x = 5.6/L_y$, and the Fourier cutoff was 5 lattice points in the x- and y-directions and 15 in the z-direction to account for $L_z \sim (3L_x = 3L_y)$. The Lennard–Jones interatomic interactions were truncated using a standard minimum image convention.

During the data collection phase of the simulations (between 60,000 and 105,000 steps), the mean density profile was collected based on Eq. (21), where the center of mass was used in designating the slab in which the molecule was situated. The virial method for surfacetension determination using polyatomic molecules followed Eq. (22), but the

expressions for the normal and tangential pressure components are slightly different [39],

$$\begin{aligned} P_{\mathrm{n}} &= \frac{1}{V}\sum_{i=1}^{N} M_i v_{\mathrm{com},iz}^2 + \frac{1}{V}\sum_{i=1}^{N}\sum_{j>i}^{N}\sum_{a=1}^{2}\sum_{b=1}^{2} F_{iajbz} z_{iabj} \\ P_{\mathrm{t}} &= \frac{1}{2V}\sum_{i=1}^{N} M_i \left(v_{\mathrm{com},ix}^2 + v_{m,iy}^2\right) \\ &\quad + \frac{1}{2V}\sum_{i=1}^{N}\sum_{j>i}^{N}\sum_{a=1}^{2}\sum_{b=1}^{2}\left(F_{iajbx} x_{iabj} + F_{iajby} y_{iabj}\right) \end{aligned} \tag{30}$$

where the net interaction between molecules i and j is the sum of the interatomic interactions and is approximated to be applied on the center of mass of those molecules. For water, the computation used Ewald summation, and the contribution of the electrostatic potentials to the x-directional pressure component follows [8, 38]:

$$\begin{aligned} P_x V &= \frac{1}{8\pi\varepsilon_0}\sum_{i=1}^{N}\sum_{a=1}^{N_{\mathrm{atom}}} q_{ia}\sum_{j\neq i}^{N}\sum_{b=1}^{N_{\mathrm{atom}}} q_{jb}\left[\frac{2}{\sqrt{\pi}}\kappa r_{iajb}\exp\left(-\kappa^2 r_{iajb}^2\right)\right. \\ &\quad \left.+\operatorname{erfc}\left(\kappa r_{iajb}\right)\right]\frac{\mathbf{x}_{ij}\mathbf{x}_{iajb}}{r_{iajb}^3} + \frac{1}{4\pi\varepsilon_0}\frac{2\pi}{V}\sum_{\mathrm{k}\neq 0} Q(k)\left|S(\mathbf{k})\right|^2\left(1-\frac{2k_x^2}{k^2}-\frac{k_x^2}{2\kappa^2}\right) \\ &\quad -\sum_{i=1}^{N}\sum_{a=1}^{N_{\mathrm{atom}}}\left(\mathbf{r}_{ia}-\mathbf{r}_i\right)\left(\mathbf{F}_{ia}^K\right)_x \end{aligned} \tag{31}$$

where $\mathbf{x}_{ij}$ is the x-vector from the center of mass of molecule i to molecule j, $\mathbf{x}_{iajb}$ is the x-vector from atom a of molecule i to atom b of molecule j, $\mathbf{r}_i$ and $\mathbf{r}_{ia}$ are the position vectors of the center of mass of molecule i and atom a of molecule i, respectively, and $\mathbf{F}_{ia}^{\mathrm{K}}$ is the Fourier component of the electrostatic force on atom a of molecule i,

$$\mathbf{F}_{ia}^{\mathrm{K}} = -\frac{q_{ia}}{4\pi\varepsilon_0}\frac{4\pi}{V}\sum_{\mathbf{k}\neq 0} Q(k)\,\mathbf{k}\,\mathrm{Im}\left\{\exp\left(-\mathbf{k}\bullet\mathbf{r}_{ia}\right)S(\mathbf{k})\right\} \tag{32}$$

The real component of the electrostatic force on atom a of molecule i is

$$\mathbf{F}_{ia}^{\mathrm{R}} = \frac{q_{ia}}{4\pi\varepsilon_0}\sum_{j\neq i}^{N}\sum_{b=1}^{N_{\mathrm{atom}}} q_{jb}\left[\frac{2}{\sqrt{\pi}}\kappa r_{iajb}\exp\left(-\kappa^2 r_{iajb}^2\right)+\operatorname{erfc}\left(\kappa r_{iajb}\right)\right]\frac{\mathbf{r}_{iajb}}{r_{iajb}^3} \tag{33}$$

The total electrostatic force on molecule i of atom a is the summation of the forces in Eqs. (32) and (33). Extension of Eq. (31) to the y- and z-directions is trivial. The normal component of pressure is then equal to the z-component, and the tangential component is the average of the x- and y-components. The system average temperature was determined from the average molecular velocities by

$$\langle T \rangle = \frac{1}{\xi N k_{\mathrm{B}}} \left\langle \sum_{i=1}^{N} \sum_{a=1}^{N_{\mathrm{atom}}} m_{ia} v_{ia}^2 \right\rangle \tag{34}$$

where m_{ia} is the mass of atom a of molecule i and ξ is the number of degrees of freedom within each molecule. The values of ξ for argon, nitrogen, and water are 3, 5, and 6, respectively.

Figures 4, 5, and 6 provide results from FEI and virial analyses for argon, nitrogen, and water, respectively. In all cases, the critical parameters

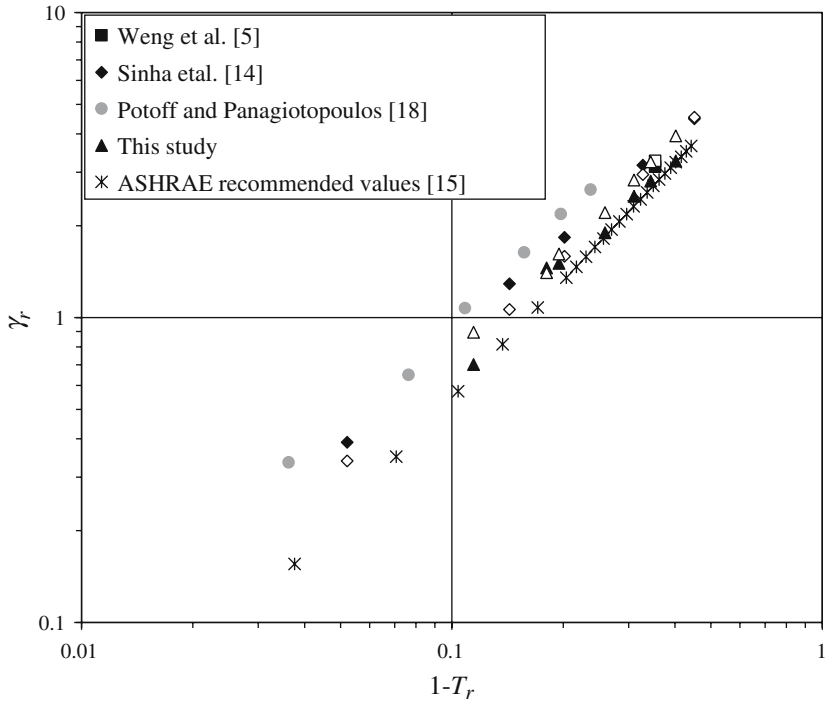

Fig. 4. Predicted surface-tension values for argon as a function of temperature using various methods. Closed black symbols represent virial method results, closed gray symbols represent finite-size method results, and open symbols represent FEI method results.

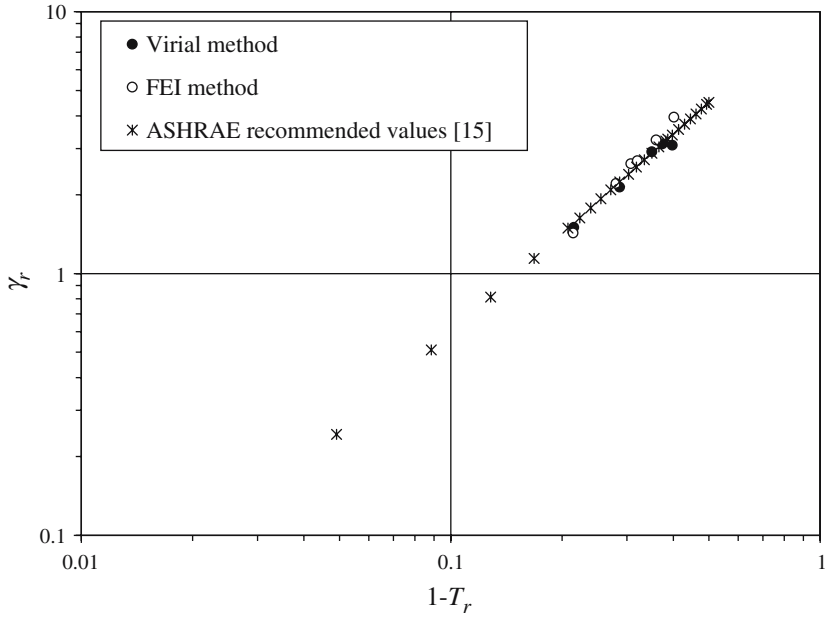

Fig. 5. Predicted surface-tension values for nitrogen as a function of temperature using the FEI and virial methods.

used in the FEI analysis were based on ASHRAE data [15], since the parameters of the intermolecular potential were chosen to model the fluid as accurately as possible for the temperature ranges given. For argon, various values of surface tension computed by the finite-size and virial methods were also taken from the literature for comparison, and the aforementioned values of the Lennard–Jones parameters were used to scale the simulation results into reduced units for comparison. In addition, the Redlich–Kwong-based FEI method was used to estimate surface tension where density profile characteristics were available. For argon, three sources were used: Wu and Pan [40], Weng et al. [5], and Sinha et al. [14]. Wu and Pan do not provide their own calculation of surface tension, but they do provide the value of the interfacial region thickness for a system at 110 K. The Weng et al. study provides its calculated value of surface tension via the virial method, while the Sinha study provides a plot of surface tension versus temperature using their modified version of the virial method. The results accredited to Sinha et al. [14] in Fig. 4 are an estimation of the surface tension values read from their plot. For all three studies, the values of bulk liquid and vapor densities were approximated from

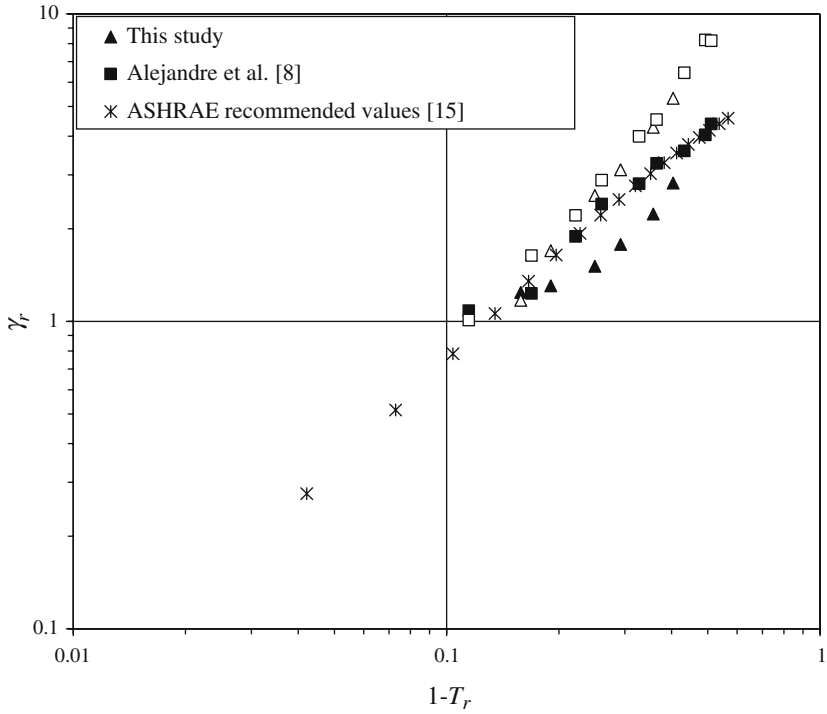

Fig. 6. Predicted surface-tension values for water as a function of temperature using the FEI and virial methods. Closed symbols represent virial method predictions, and open symbols represent FEI method predictions.

the provided plots of the density profile through the interfacial region. In the Weng et al. and Sinha et al. studies, the values of the interfacial region thickness used in the post-simulation analyses were approximated from density profile plots provided by these studies by tracing a line tangent to the density profile at $\rho = \rho_m$. The results show that all methods exhibit the correct trends with the ASHRAE data, and the FEI method predicts values approximately 25% greater than the ASHRAE data and 10% less than the finite-size scaling data.

The nitrogen results, plotted in Fig. 5, show that both the virial and FEI methods agree with the ASHRAE results within 7.5%. For water, the FEI method was applied to the MD simulations of this study and the results of SPC/E water simulations provided by Alejandre et al. [8]. Their study provided values of the interfacial region thickness, the bulk densities, and the calculated surface tension by the virial method as a function of

temperature. The predicted values of surface tension by the FEI method are nearly identical using simulation data provided by this study or by Alejandre et al. [8]. The agreement between the FEI method results and the ASHRAE data increases with temperature, and thus works best for reduced temperatures higher than 0.7. It should be noted that the surface-tension values derived for SPC/E water via the virial method in Fig. 6 did not compare as well to the ASHRAE recommended values as those generated by Alejandre et al. [8].

For water, the FEI predictions were 50% higher than the ASHRAE recommended values for low temperatures, but the deviation was less than 30% for $T_r > 0.7$. Carey's [22] investigation suggested that predicting surface tension by determining the net excess free energy per unit area using a Redlich–Kwong fluid model should contain an error of approximately 30% from the ASHRAE recommended values. Furthermore, Binder and Muller [20] have suggested that the predicted density profiles for water systems are strongly influenced by domain size and disagree with experiments [41], so caution should be exercised when applying the FEI method to interfaces containing polar molecules. Nevertheless, the results shown in Fig. 6 suggest that the water surface tension predictions using the FEI method provide good agreement with ASHRAE data for reduced temperatures above 0.7.

5. APPLICATION TO EXPERIMENTALLY DETERMINED VALUES OF THICKNESS

The FEI method can be used to compute the interfacial tension if values of the interfacial region thickness are available. In some instances, this can provide a useful means of predicting the interfacial tension for conditions under which it is difficult to measure directly. An example is determination of the interfacial tension at temperatures approaching the critical point using experimentally measured interfacial region thickness data.

In order to use the FEI method, values of the bulk densities must be approximated. Asymptotic analysis of the Redlich–Kwong model predicts that the difference between the saturated liquid and vapor densities is [23]

$$\frac{\rho_l - \rho_v}{\rho_c} = 5.15\,(1 - T_r)^{0.5} \tag{35}$$

Equation (35) can be rearranged into the form

$$\left(\rho_{r,l} - 1\right) + \left(1 - \rho_{r,v}\right) = 5.15\,(1 - T_r)^{0.5} \tag{36}$$

Carey [22] provides 6 reduced saturated liquid and vapor density values for a Redlich–Kwong fluid with $T_r \geq 0.9$. Fit curves to these data exhibit the tendencies,

Table III. Calculated Surface Tension Values for Sulfur Hexafluoride Using Density Values from Eqs. (32a) and (32b) and Interfacial Region Thickness Values from Beysens and Robert [42]

$1-T_r$	$\delta\zeta_i$	$\rho_{r,l}$	$\rho_{r,v}$	$\gamma_r=\gamma/(P_c L_i)$
0.0010	71.2	1.107	0.941	0.0010
0.0013	66.4	1.119	0.935	0.0014
0.0015	56.9	1.131	0.928	0.0019
0.0019	47.0	1.147	0.919	0.0028
0.0025	37.5	1.169	0.908	0.0042
0.0030	37.0	1.183	0.900	0.0053
0.0035	28.9	1.199	0.891	0.0068
0.0040	27.5	1.213	0.883	0.0081
0.0044	33.2	1.224	0.877	0.0093
0.0048	29.4	1.233	0.872	0.0104
0.0055	28.9	1.250	0.863	0.0127

$$\left(\rho_{r,l}-1\right)\approx 3.37\,(1-T_r)^{0.5} \tag{37a}$$

$$\left(1-\rho_{r,v}\right)\approx 1.85\,(1-T_r)^{0.5} \tag{37b}$$

Note that adding Eqs. (37a) and (37b) produce the relation of Eq. (36) with an error of less than 2%.

The methodology described above was used to predict γ_r values for sulfur hexafluoride very close to the critical point. Beysens and Robert [42] used optical reflectivity measurements to determine values of interfacial region thickness for sulfur hexafluoride as a function of temperature at near-critical conditions. Equations (37a) and (37b) were used to approximate the bulk liquid and vapor densities for each temperature, and the FEI method was used to predict the surface tension from these interfacial region values. The values of the interfacial region thickness, reduced bulk densities, and derived surface tension are listed in Table III.

Figure 7 shows calculated values of surface tension using the FEI method and the expected surface tension trend based on an approximated datum. This datum applies vapor–pressure data by Verdelli et al. [43] along with critical values recommended by Horvath [44] into relations given by Riedel [45, 46]. The expected trend given by the figure stems from the vanishing of surface tension as the system approaches the critical point and the known Ising model power-law variation usually observed for pure fluids [16] as the temperature is increased towards the critical point: $\gamma \sim (1-T_r)^{1.26}$. Although the magnitude of the derived surfacetension values are lower than the expected trend, the consistency of this observed trend

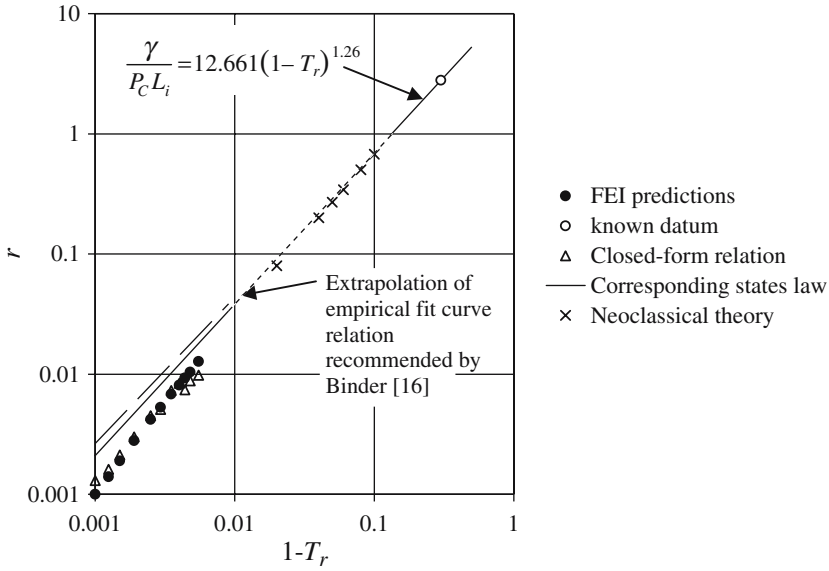

Fig. 7. Comparison of surface-tension values found using the FEI method with the empirically fitted trend to an approximated datum. Derived values were based on recommended interfacial thickness values from Beysens and Robert [42] and vapor pressure data by Verdelli et al. [43]. Datum was found using methods by Riedel [45, 46] and vapor–pressure data by Verdelli et al. [43]. Also shown are predictions by the closed-form relation [23], and trends predicted by the neoclassical theory [22] and the corresponding-states law [21].

with this expected variation provides some confirmation that the surface tension values computed with this analysis are reliable predictions of this property. Also shown are predicted values by the closed-form relation by Carey and Wemhoff [23],

$$\gamma_{\mathrm{r}} = 1.5764 \left[\frac{(1-T_{\mathrm{r}})^{-0.34}}{T_{\mathrm{r}}^{1/2}} \right] \ln \left[\frac{1+0.26\rho_{\mathrm{r,l}}}{1+0.26\rho_{\mathrm{r,v}}} \right] \left(\frac{\rho_{\mathrm{r,l}} - \rho_{\mathrm{r,v}}}{\delta \zeta_i} \right) \tag{38}$$

Figure 7 also shows predictions via the neoclassical theory of capillarity [22] and the power-law variation predicted by the corresponding states law [21]. The figure shows that the FEI predictions strongly agree with those by the closed-form relation, and the trend exhibited by the data follow that by the corresponding states law, the neoclassical theory, and the Ising model. At the highest temperature, the FEI prediction disagrees with the Ising model by approximately 50%.

6. CONCLUDING REMARKS

The FEI method presented here provides a simple means of estimating surface tension from a knowledge of the system temperature and density profile characteristics. The strength of this method lies in the fact that it links the interfacial tension to the thickness of the interfacial region, and it is tunable to a wide variety of fluids. For nonpolar fluids, the results from the Redlich–Kwong-based FEI method provide reasonable agreement with ASHRAE thermodynamic data for the conditions set for our MD simulations. This good agreement exists because nonpolar fluids are well-approximated by the Redlich–Kwong fluid model. For water, the FEI method provides reasonable agreement with ASHRAE recommended values for reduced temperatures greater than 0.7. The Redlich–Kwong fluid model does not match water well for lower temperatures when the effects of polarity are more prominent, and a more suitable fluid model may provide better agreement.

APPENDIX: LOCAL FREE ENERGY DENSITY CALCULATION USING THE REDLICH–KWONG FLUID MODEL

The partition function was previously developed using Rayleigh's model to account for the density gradient and the Redlich–Kwong model for fluid properties [22, 23]:

$$\begin{aligned}\ln Q = N + \left(\frac{3N}{2}\right)\ln\left[\frac{2\pi M k_{\mathrm{B}} T\,(V - N b_{\mathrm{R}})^{2/3}}{N^{2/3} h^2}\right] + N\left[\frac{\xi - 5}{2}\ln\pi - \ln\sigma_{\mathrm{s}}\right] \\ + \frac{\xi - 3}{2} N \ln\left(\frac{T}{\theta_{\mathrm{rot},m}}\right) + \frac{a_{\mathrm{R}0} N}{b_{\mathrm{R}} k_{\mathrm{B}} T^{3/2}}\ln\left(\frac{V + N b_{\mathrm{R}}}{V}\right) \\ + \frac{a_{\mathrm{R}0}\kappa V \rho''}{2 b_{\mathrm{R}} k_{\mathrm{B}} T^{3/2}}\ln\left(\frac{V + N b_{\mathrm{R}}}{V}\right)\end{aligned} \tag{A1}$$

where M is the molecular mass, N is the number of molecules in a volume V, ρ is the number density $= N/V$, a_{R0} and b_R are the Redlich–Kwong coefficients, k_B is Boltzmann's constant, T is temperature, h is Planck's constant, ξ is the number of degrees of freedom of the molecule, σ_{s} is the symmetry number, $\theta_{\mathrm{rot},m}$ is the rotational temperature of mode m, and κ is the parameter,

$$\kappa = \frac{-\frac{2\pi}{3}\displaystyle\int_{r_{\min}}^{r_{\max}} \phi(r) r^4 dr}{-2\pi \displaystyle\int_{r_{\min}}^{r_{\max}} \phi(r) r^2 dr} \tag{A2}$$

where $\phi(r)$ is the potential energy interaction between a molecule and the surrounding fluid at a radius r. Note that the Redlich–Kwong equation of state can be determined from Eq. (A1) for zero curvature $\left(\rho''=0\right)$ by

$$P=k_{\mathrm{B}}T\left(\frac{\partial \ln Q}{\partial V}\right)_{T,N}=\frac{Nk_{\mathrm{B}}T}{V-b_{\mathrm{R}}N}-\frac{a_{\mathrm{R0}}N^2}{T^{1/2}V\left(V+b_{\mathrm{R}}N\right)} \tag{A3}$$

The Redlich–Kwong coefficients a_{R0} and b_{R} may be found at the inflection along the P–v curve of the equation of state (A3) at the critical point [47] to yield

$$a_{\mathrm{R0}}=0.42748\frac{k_{\mathrm{B}}^2T_{\mathrm{c}}^{2.5}}{P_{\mathrm{c}}} \tag{A4}$$

$$b_{\mathrm{R}}=0.08664\frac{k_{\mathrm{B}}T_{\mathrm{c}}}{P_{\mathrm{c}}} \tag{A5}$$

The free energy density can be calculated from the partition function by

$$\psi=\frac{F}{V}=-\frac{k_{\mathrm{B}}T}{V}\ln Q \tag{A6}$$

where F is the Helmholtz free energy for a mass of fluid of volume V. Combining Eqs. (A1) and (A6) yields

$$\begin{aligned}\psi=&-\rho k_{\mathrm{B}}T-\left(\frac{3\rho k_{\mathrm{B}}T}{2}\right)\ln\left[\frac{2\pi Mk_{\mathrm{B}}T\left(1-\rho b_{\mathrm{R}}\right)^{2/3}}{\rho^{2/3}h^2}\right]-\rho k_{\mathrm{B}}T\left[\frac{\xi-5}{2}\ln\pi-\ln\sigma_{\mathrm{s}}\right]\\&-\rho k_{\mathrm{B}}T\left(\frac{\xi-3}{2}\right)\ln\left(\frac{T}{\theta_{\mathrm{rot},m}}\right)-\frac{a_{\mathrm{R0}}\rho}{b_{\mathrm{R}}T^{1/2}}\ln\left(1+\rho b_{\mathrm{R}}\right)\\&+\frac{a_{\mathrm{R0}}\kappa\rho''}{2b_{\mathrm{R}}T^{1/2}}\ln\left(1+\rho b_{\mathrm{R}}\right)\end{aligned} \tag{A7}$$

The value of κ is given by [22, 23]

$$\kappa=\frac{-\frac{2\pi}{3}\int_{r_{\min}}^{r_{\max}}\phi\left(r\right)r^4dr}{-2\pi\int_{r_{\min}}^{r_{\max}}\phi\left(r\right)r^2dr}=L_i^2 0.1613\left(1-T_{\mathrm{r}}\right)^{-0.34}, \tag{A8}$$

Substituting Eq. (A8) into Eq. (A7) yields

$$\begin{aligned}\psi=&-\rho k_{\mathrm{B}}T\left\{\frac{3}{2}\ln\left[\frac{\left(1-\rho b_{\mathrm{R}}\right)^{2/3}}{\rho^{2/3}\Lambda^2}\right]+F_1\right\}-\frac{a_{\mathrm{R0}}\ln\left(1+\rho b_{\mathrm{R}}\right)}{b_{\mathrm{R}}T^{1/2}}\\&\times\left[\rho+L_i^2 0.08065\left(1-T_{\mathrm{r}}\right)^{-0.34}\rho''\right]\end{aligned} \tag{A9}$$

where

$$\Lambda = \left[\frac{h^2}{2\pi M k_B T} \right]^{1/2} \tag{A10}$$

and

$$F_1 = 1 + \frac{\xi - 5}{2} \ln\pi - \ln\sigma_s + \left(\frac{\xi - 3}{2} \right) \ln\left(\frac{T}{\theta_{rot,m}} \right) \tag{A11}$$

NOMENCLATURE

a_{R0}	Redlich–Kwong constant for zero density gradient
b_R	Redlich–Kwong constant
k_B	Boltzmann constant
L_i	interfacial region characteristic length
M	molecular mass
m	atomic mass
N	number of molecules
N_{atom}	number of atoms per molecule
N_A	Avogadro's number
P	pressure
q	point charge value
Q	partition function
R	universal gas constant
T	temperature
V	system volume
z	coordinate normal to the interface
δz_i	interfacial region thickness
ε	Lennard–Jones energy parameter
ε_0	permittivity of vacuum
γ	interfacial tension
ξ	number of translational plus rotational energy storage modes
ρ	number density of molecules
σ	Lennard–Jones parameter
$\theta_{rot,m}$	mean rotational temperature
ϕ_{ij}	intermolecular potential
ζ	nondimensional interfacial region position
ε_{rot}	rotational energy
F_{ij}	intermolecular force
h	Planck's constant

F	Helmholtz free energy
ψ	Helmholtz free energy density
σ_s	symmetry number

Subscripts

bin	bin volume
c	critical point property
com	center of mass
l	saturated bulk liquid
m	mean of saturated bulk liquid and vapor properties
n	normal component
v	saturated bulk vapor
r	reduced property (normalized with critical properties)
sat	saturation property
t	tangential component

REFERENCES

1. B. B. Mikic and W. M. Rohsenow, *J. Heat Trans*. **91**:245 (1969).
2. C. Graham and P. Griffith, *Int. J. Heat Mass Trans*. **16**:337 (1973).
3. E. K. Ungar, I. Y. Chen, and S. H. Chan, *Proc. 7th AIAA/ASME Joint Thermophysical and Heat Trans. Conf., HTD* **357:** 71 (1988).
4. J. G. Kirkwood and F. P. Buff, *J. Chem. Phys.* **17**:338 (1949).
5. J. G. Weng, S. Park, J. R. Lukes, and C. L. Tien, *J. Chem. Phys*. **113**:5917 (2000).
6. S. Enders, H. Kahl, M. Mecke, and J. Winkelmann, *J. Mol. Liquids* **115**:29 (2004).
7. J. G. Harris, *J. Phys. Chem.* **96**:5077 (1992).
8. J. Alejandre, D. J. Tildesley, and G. A. Chapela, *J. Chem. Phys*. **102**:4574 (1995).
9. M. J. P. Nijmeijer, A. F. Bakker, C. Bruin, and J. H. Sikkenk, *J. Chem. Phys*. **89**:3789 (1988).
10. D. O. Dunikov, S. P. Malyshenko, and V. V. Zhakhovskii, *J. Chem. Phys*. **115**:6623 (2001).
11. C. D. Holcomb, P. Clancy, and J. A. Zollweg, *Mol. Phys*. **78**:437 (1993).
12. M. Mecke, J. Winkelmann, and J. Fischer, *J. Chem. Phys*. **107**:9264 (1997).
13. J. A. Barker, *Mol. Phys*. **80**:815 (1993).
14. S. Sinha, V. K. Dhir, B. Shi, J. B. Freund, and E. Darve, *Proc. 2003 ASME Summer Heat Trans. Conf.* (2003).
15. *ASHRAE Fundamentals Handbook* (American Society of Heating, Refrigerating, and Air-conditioning Engineers, Atlanta Georgia, 2001).
16. K. Binder, *Phys. Rev. A* **25**:1699 (1982).
17. J. Errington, *Phys. Rev. E* **67**:012102 (2003).
18. J. Potoff and A. Panagiotopoulos, *J. Chem. Phys*. **112**:6411 (2000).
19. J. Hunter and W. Reinhardt, *J. Chem. Phys*. **103**:8627 (1995).
20. K. Binder and M. Muller, *Int. J. Mod. Phys. C* **11**:1093 (2000).
21. J. R. Brock and R. B. Bird, *AIChE J*. **1**:174 (1955).
22. V. P. Carey, *J. Chem. Phys*. **118**:5053 (2003).
23. V. P. Carey and A. P. Wemhoff, *Int. J. Thermophys.* **25**:753 (2004).

24. J. Rowlinson and B. Widom, *Molecular Theory of Capillarity* (Clarendon Press, Oxford, 1982).
25. J. D. van der Waals, *On the Continuity of the Gaseous and Liquid States*, in *Studies in Statistical Mechanics*, Vol. 14 (North Holland, Amsterdam, 1988).
26. S. Fisk and B. Widom, *J. Chem. Phys*. **50**:3219 (1969).
27. F. P. Buff, R. A. Lovett, and F. H. Stillinger, *Phys. Rev. Lett*. **15**:621 (1965).
28. M. Robert and C. Stuart, *Phys. Rev. Lett*. **49**:1434 (1982).
29. M. Robert, *Phys. Rev. B* **30**:6666 (1984).
30. A. P. Wemhoff, *Ph. D. Dissertation* (University of California at Berkeley, 2004).
31. G. E. P. Box and M. E. Mueller, *Ann. Math. Stat*. **29**:610 (1958).
32. M. P. Allen and D. J. Tildesley, *Computer Simulation of Liquids* (Clarendon Press, Oxford, 1987).
33. C. L. Tien and J. G. Weng, *Adv. App. Mech.* **38**:95 (2001).
34. V. P. Carey and N. E. Hawks, *J. Heat Trans*. **117**:432 (1995).
35. H. C. Andersen, *J. Comput. Phys*. **52**:24 (1983).
36. J. Fischer, R. Lustig, H. Breitenfelder-Manske, and W. Lemming, *Mol. Phys*. **52**:485 (1984).
37. H. J. C. Berendsen, J. R. Grigera, and T. P. Straatsma, *J. Chem. Phys*. **91**:6269 (1987).
38. D. M. Heyes, *Phys. Rev. B* **49**:755 (1994).
39. G. Ciccotti and J. P. Ryckaert, *Comp. Phys. Rep*. **4**:348 (1986).
40. Y. W. Wu and C. Pan, *Proc. ASME 2003 Summer Heat Trans. Conf*. (2003).
41. M. Matsumoto and Y. Kataoka, *J. Chem. Phys*. **88**:3233 (1988).
42. D. Beysens and M. Robert, *J. Chem. Phys.* **87**:3056 (1987).
43. L. S. Verdelli, H. C. Miller, and J. F. Gall, *Ind. Eng. Chem.* **43**:1126 (1951).
44. A. L. Horvath, *Physical Properties of Inorganic Compounds* (Crane Russak, New York, 1975).
45. L. Riedel, *Chem. Ing. Tech.* **26**:83 (1954).
46. L. Riedel, *Chem. Ing. Tech.* **27**:209 (1955).
47. R. Reid, J. M. Prausnitz, and B. E. Poling, *Properties of Gases and Liquids* (McGraw-Hill, New York, 1987).